arXiv:2009.11161v1 [cond-mat.mes-hall] 23 Sep 2020

# Indium gallium nitride quantum dots: Consequence of random alloy fluctuations for polarization entangled photon emission

**Saroj Kanta Patra**[1,2] **& Stefan Schulz**[1]

[1] Tyndall National Institute, University College Cork, Cork, Ireland
[2] Department of Electrical Engineering, University College Cork, Cork, Ireland

E-mail: sarojkanta.patra@tyndall.ie

1 March 2024

**Abstract.** We analyze the potential of the *c*-plane InGaN/GaN quantum dots for polarization entangled photon emission by means of an atomistic many-body framework. Special attention is paid to the impact of random alloy fluctuations on the excitonic fine structure and the excitonic binding energy. Our calculations show that *c*-plane InGaN/GaN quantum dots are ideal candidates for high temperature entangled photon emission as long as the underlying $C_{3v}$-symmetry is preserved. However, when assuming random alloy fluctuations in the dot, our atomistic calculations reveal that while the large excitonic binding energies are only slightly affected, the $C_{3v}$ symmetry is basically lost due to the alloy fluctuations. We find that this loss in symmetry significantly impacts the excitonic fine structure. The observed changes in fine structure and the accompanied light polarization characteristics have a detrimental effect for polarization entangled photon pair emission via the biexciton-exciton cascade. Here, we also discuss possible alternative schemes that benefit from the large excitonic binding energies, to enable non-classical light emission from *c*-plane InGaN/GaN quantum dots at elevated temperatures.

## 1. Introduction

Non-classical light sources capable of efficiently emitting entangled photon pairs is one of the basic requirements to realize secure quantum communication [1, 2, 3]. Several methods have been employed in the past to realize highly efficient entangled photon sources [4, 5]. For instance, parametric down conversion of atomic based systems is one of the widely used method in this regard. [6, 7] However, photon generation through this scheme is probabilistic and reduces the overall efficiency. [3] For this reason, semiconductor quantum dots (QDs) have been a topic of enormous scientific research interest in recent years, since in principle they can generate polarization entangled photon pairs deterministically by utilizing the biexciton-exciton cascade [8, 9]. The underlying concept in an *ideal* structure is schematically illustrated in Fig. 1 (a). Using this cascade and having a degenerate bright excitonic (ground) state of energy $E_X$, the photons emitted will be polarization entangled [10]:

$$|\psi\rangle = \frac{1}{\sqrt{2}}\left(|\sigma^+_{XX}\sigma^-_X\rangle + |\sigma^-_{XX}\sigma^+_X\rangle\right) \ . \qquad (1)$$

Here, $\sigma^{\pm}_{XX}$ ($\sigma^{\pm}_X$) indicates that the emitted biexciton (exciton) photon is left/right circularly polarized. [10]

This scheme has been heavily studied using zincblende (ZB) InGaAs/GaAs QDs grown along the crystallographic [001]-direction. [11, 12] However, early investigations revealed that this idealized picture of degenerate bright excitonic states is not fulfilled due to the overall $C_{2v}$ symmetry of the combined system of QD geometry and underlying ZB crystal structure. [13] Even in an idealized dot geometry (e.g. square-based pyramid), the $C_{2v}$ symmetry lifts the degeneracy of bright excitonic states, resulting in a so-called fine structure splitting (FSS), $\Delta_{\mathrm{FSS}}$. A schematic illustration of this situation is depicted in Fig. 1. This small FSS (several tenth of $\mu$eV) leads also to a change in the light polarization characteristics of the emitted photons; the photons are linearly polarized, here labeled as vertical (V) and horizontal (H) to a given reference axis. However, it should be noted that even in the presence of a non-vanishing FSS, in principle, an "entangled" photon state can be realized via [4]:

$$|\psi\rangle = \frac{1}{\sqrt{2}}\left(|H_{XX}H_X\rangle + e^{\frac{i\cdot\Delta_{\mathrm{FSS}}\cdot\tau}{\hbar}}|V_{XX}V_X\rangle\right) \ , \qquad (2)$$

where $e^{\frac{i\cdot\Delta_{\mathrm{FSS}}\cdot\tau}{\hbar}}$ is a phase factor which depends on the product of FSS and exciton lifetime $\tau$. If $\Delta_{\mathrm{FSS}}$ is smaller than the excitonic emission linewidth or $\tau$ is very small so that product $\frac{\Delta_{\mathrm{FSS}}\cdot\tau}{\hbar} \approx 0$, an entangled photon pair can be obtained. [10]

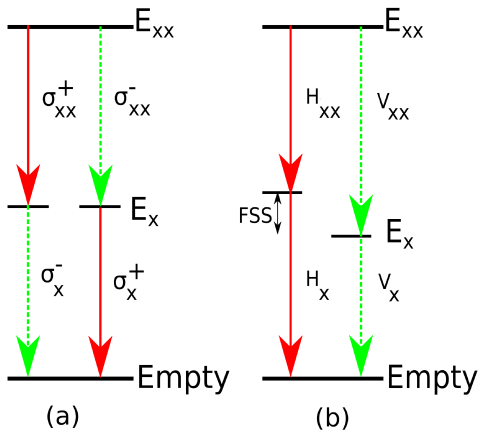



**Figure 1.** Schematic illustration of the light polarization properties of photons emitted from a biexciton-exciton cascade. (a) Vanishing fine structure splitting $\Delta_{\mathrm{FSS}} = 0$. In this case the photons are circularly ($\sigma_{\pm}$) polarized. (b) Non-vanishing fine structure splitting, the emitted photons are linearly polarized, either horizontally (H) or vertically (V) to a given reference axis.

Thus, it is of key importance to find systems that either have intrinsically a small FSS or in which the FSS can tuned to be close to zero. The latter has been addressed in the literature by applying external electric or piezoelectric fields. [10] Overall, given that the FSS is tightly linked to the symmetry of the combined system of dot geometry and underlying crystal structure, in ZB QDs growth along different crystallographic directions has been targeted. For ZB InGaAs/GaAs dots, growth along the [111]-direction has generated significant interest, since the underlying symmetry is $C_{3v}$ if the QD is for instance lens-shaped or a (truncated) pyramid with a triangular base; in a $C_{3v}$-symmetric system the FSS vanishes. [12, 13] For [111]-oriented InGaAs/GaAs dots this has already been demonstrated in the literature [14].

While InGaAs/GaAs dots, especially when grown along the [111]-direction, have been widely studied, material intrinsic properties such as the small band offsets limit their application to low temperatures. An attractive alternative to these *ZB* arsenide-based systems are *wurtzite* (WZ) *c*-plane III-N QDs, utilizing InN, GaN, AlN and their respective alloys. Ideally, such *c*-plane III-N dots should also exhibit a $C_{3v}$ symmetry. [15, 16] Additionally, valence and conduction band offsets between III-N materials are very large ($\geq$ 500 meV between the binary materials). [17] Moreover it has been shown that exciton binding energies are very large ($\geq$30 meV) in III-N dots. [18, 19] Thus, these intrinsic properties are indicative of bringing entangled photon emission near room temperature within reach. Non-classical light emission via single-photon emission above 200 K has already been demonstrated in the literature for III-N dots. [20, 21, 22] However, compared to InGaAs/GaAs QDs, entangled photon emission from III-N has been studied far less and if so mainly for GaN/AlN dots,

thus for emission in the UV spectral region. [23] When using InGaN/GaN dots, the additional benefit of an in principle flexible emission wavelength engineering in the visible spectral range is possible, while ideally keeping all other benefits ($C_{3v}$ symmetry, large band offsets, large excitonic binding energies). However, the study of the potential of InGaN/GaN QDs for entangled photon emission is sparse, and even when studied theoretically the question of atomistic effects arising from alloy fluctuations in InGaN is not addressed. However, it is important to note that the optical properties of InGaN/GaN quantum wells are strongly affected by alloy fluctuations. [24, 25]

Here, we present a detailed theoretical analysis of the electronic and optical properties of *c*-plane InGaN/GaN QDs by means of an atomistic many-body theoretical framework. This framework allows us to study the impact of random alloy fluctuations on both the electronic structure and the excitonic FSS. We discuss resulting consequences for entangled photon emission from *c*-plane InGaN/GaN dots at elevated temperatures.

Our results show that when InGaN/GaN dots preserve a $C_{3v}$ symmetry, they are very promising candidates for producing polarization-entangled photon pairs at high temperatures. For instance, in an idealized truncated cone shaped InGaN/GaN dot system, we observe a zero FSS between bright excitonic states and an excitonic binding energy of approximately 50 meV. While when including random alloy fluctuations in the description the excitonic binding energies are still very large (>35 meV), and even when keeping the truncated-cone shaped dot geometry, we find that the random alloy fluctuations break the $C_{3v}$-symmetry. This symmetry breaking significantly changes the excitonic fine structure, which as we will show, has a detrimental effect for polarization entangled photon emission; emitted photons are not orthogonally polarized. Therefore, controlling the symmetry of *c*-plane InGaN/GaN QDs will be key to use these dot systems for polarization entangled photon emission at elevated temperatures. We will also briefly discuss how entanglement may still be possible through alternative schemes. Overall, with the added advantage of high exciton binding energies and tunable emission wavelength, and when controlling the symmetry of the system, *c*-plane InGaN/GaN dots are potential candidate for high temperature non-classical light emission over a wide wavelength range.

The paper is organized as follows. We start in Sec. 2 with a brief discussion of the theoretical framework. The full details are given in an Appendix. Section 3 presents the QD geometry used in this study. In Sec. 4.1 we analyze the impact of alloy fluctuations on the single particle states and energies, while in Sec. 4.2 the excitonic FSS, excitonic binding energies and light polarization characteristics of the emitted photons are presented and analyzed. In all these investigations special attention is paid to the impact of random alloy fluctuations on the results. Finally, we summarize our work in Sec. 5.

## 2. Theoretical framework

In this section we briefly describe the theoretical background underlying our calculations of electronic and optical properties of *c*-plane InGaN/GaN QDs. More details of the underlying methods can be found the Appendix.

On the electronic structure side we apply an $sp^3$ tight-binding (TB) model. Since our aim is to understand the impact of alloy fluctuations in detail, we use two different frames for the TB model, namely a fully atomistic description and a virtual crystal approximation (VCA). In the VCA approach we neglect any alloy fluctuations and assume that the atoms in the dot region can be described by virtual atoms, for which the corresponding TB parameters are obtained as average of the TB parameters for InN and GaN. Of central importance is that the VCA description preserves the $C_{3v}$ symmetry of the system (see discussion below on QD geometry). For the fully atomistic case we resolve alloy fluctuations in the system, and set the TB parameters according to the local atomic species. Both VCA and atomistic framework account for strain and built-in fields. In the VCA case a continuum-based description via a surface integral method is applied, [26] while in the microscopic description strain and built-in fields are determined from valence force field and local polarization theory methods. [27]

Since the evaluation of the excitonic properties is intrinsically a many-body problem, we employ the configuration interaction (CI) scheme. [15, 28] The CI scheme allows us to account for electron-hole exchange interaction effects, important for the description of the excitonic FSS, $\Delta_{\mathrm{FSS}}$, and takes as input the TB single-particle energies and Coulomb matrix elements calculated from TB wave functions. Using Fermi's golden rule, and calculating dipole matrix elements from TB wave functions, insight into polarization resolved excitonic emission and absorption spectra is gained.

Overall, our chosen theoretical framework allows us to study how deviations from an ideally $C_{3v}$ symmetric system due to alloy fluctuations will affect both electronic and optical properties. Additionally, equipped with information about quantities such as exciton binding energy, FSS and light polarization characteristics, we will discuss the potential of *c*-

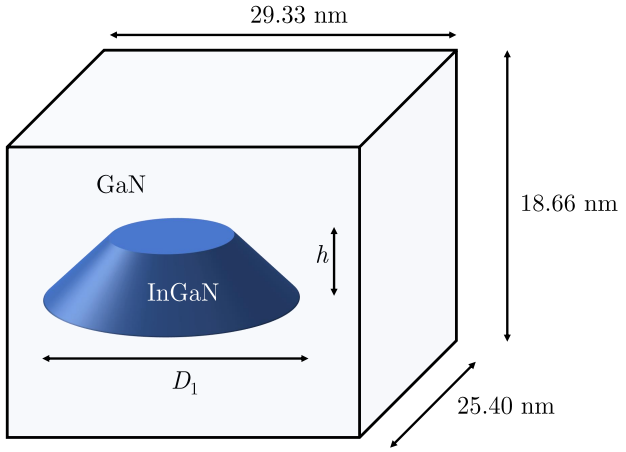



**Figure 2.** Schematic illustration of a truncated-cone shaped $c$-plane InGaN QD buried in a GaN matrix considered in this study. The diameter (height) of the QD is denoted by $D_1$ ($h$). Additionally, the supercell dimensions are given; the considered system contains 1,218,816 atoms

plane InGaN/GaN QDs for (elevated temperature) entangled photon emission. In order to perform these studies, the model needs as input (i) the QD size and geometry, and (ii) for the fully atomistic description the In atom distribution in the dot. We also note that when studying the electronic structure and optical properties, and in particular the FSS, of $c$-plane WZ QDs, the choice (symmetry) of the supercell is extremely important. If the latter aspect is not carefully considered, the FSS values predicted are potentially too large. All these aspects will be discussed in the following section.

## 3. Quantum dot geometry, simulation supercell and alloy configurations

As mentioned above, the theoretical framework requires QD geometry and size as an input as well as the In content. Recent structural investigations on $c$-plane InGaN QDs, [29] using transmission electron microscopy (TEM), revealed truncated cone-shaped geometries for such dots. The reported dot diameter are in the range of ≈10-20 nm, with heights varying between 3-5 nm. [29] The In content of experimentally realized InGaN/GaN dots is typically in the 20% to 25% range. [30, 31] Building on these recent experimental results, we have assumed a truncated-cone shaped InGaN QD with a base diameter $D_1$= 13 nm and a height $h$ = 3 nm; the In content of our dot is 20%. The QD geometry is schematically shown in Fig. 2. Previous theoretical studies on $c$-plane InGaN QDs have also assumed similar geometries [32, 33].

Having established information about the general shape, size and (average) In content, in the fully atomistic description, also the In atom distribution in the dot region is required. For $c$-plane InGaN/GaN quantum well structures, experimental atom probe tomography studies reveal that the In atom distribution reflects that of a random alloy. [34, 35] Therefore, in a truncated cone-shaped area of the simulation cell, Ga atoms are replaced randomly by In atoms.

For the VCA calculations, this microscopic feature is lost, since within the dot all atoms are treated as virtual atoms, described by TB parameters interpolated between InN and GaN TB parameters. The virtual atoms are placed on an ideal WZ lattice. Therefore, due to the dot geometry and the VCA description, the symmetry of the system is in principle $C_{3v}$. However, care must be taken when generating a supercell for the calculation of electronic and optical properties. [36] Ideally, and to preserve the $C_{3v}$ symmetry, the supercell could for instance be hexagonal, so that a rotation of 120° around the $c$-axis/$z$-axis is a symmetry operation of the system. Our supercell is of rectangular shape, which in principle breaks this symmetry; thus this may lead to artifacts in the calculated FSS. However, given that we are interested in bound single-particle states, for which the wave functions quickly decay away from the dot, we use large supercells so that the boundary conditions do not impact the electronic and optical properties of the dot; similar approaches have been discussed by other groups. [37] We will revisit this aspect in more detail below. The dimensions of our supercell are ≈(29.33 nm×25.40 nm×18.66 nm (1218816 atoms) with periodic boundary conditions.

## 4. Results and discussion

In this section we present the results of our calculations. We start with an analysis of the single-particle states and energies in Sec. 4.1. We discuss initially the VCA results, Sec. 4.1.1, followed by an investigation of the impact of random alloy fluctuations on the electronic structure, Sec. 4.1.2. In Sec. 4.2, we study the excitonic fine structure and light polarization characteristics of the dot emission using the VCA, Sec. 4.2.1. Subsequently, the impact of alloy fluctuations on these quantities is analyzed, Sec. 4.2.2. These studies are accompanied by group theoretical arguments shedding further light onto the determined results.

### *4.1. Single particle states and energies*

We start the discussion with the VCA results of the single-particle electron and hole states. Using group theory, we also make general statements about the electronic structure in terms of (expected) degeneracies of energy levels and classify the different single-particle states according to irreducible representation (IRRs).

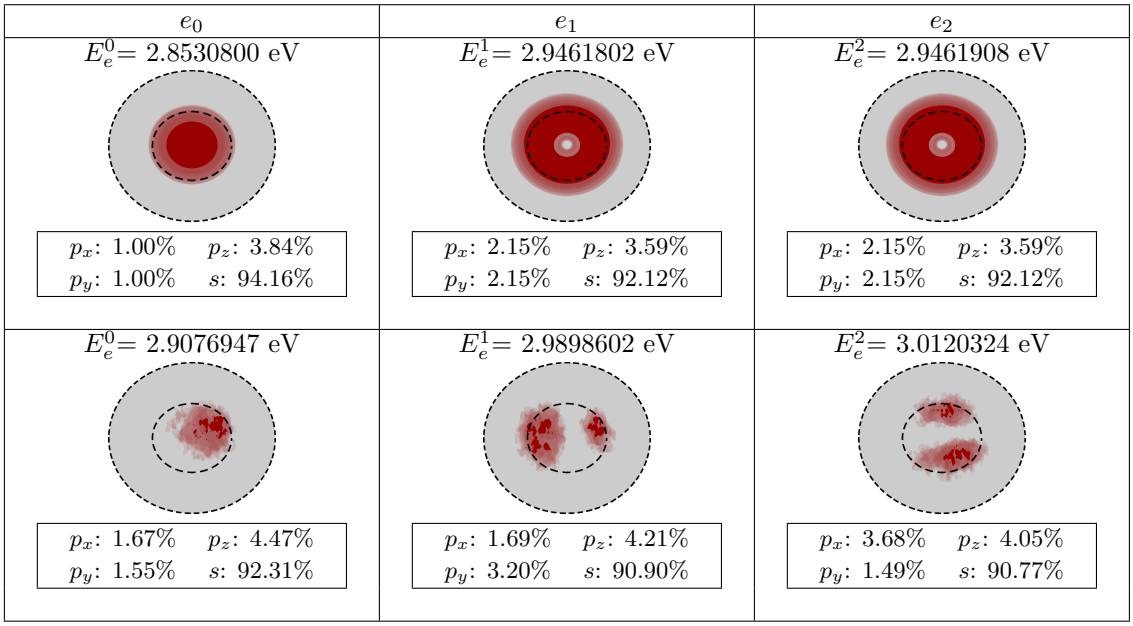



**Figure 3.** Isosurface plots of the single-particle charge densities of the energetically lowest three electron states ($e_0$: ground state; $e_1$: first excited state; $e_2$: second excited state) of a $c$-plane $In_{0.20}Ga_{0.80}N$/GaN QD. The light (dark) red isosurface corresponds to 10% (50%) of the respective maximum charge densities. The different sub-figures give also the single-particles energies $E_e^i$ and the ($s$, $p_x$, $p_y$, $p_z$) orbital contributions (in percent). Upper row: Results for a virtual crystal approximation. Lower row: Same as in the upper row but when random alloy fluctuations are described on an atomistic level. All calculations include strain and built-in field effects as well as spin-orbit coupling. Each single particle state is two-fold Kramers degenerate.

The latter is useful for understanding and explaining the calculated exciton fine structure. In a second step we study the impact of the alloy fluctuations on the results.

*4.1.1. Virtual crystal approximation* The upper row of Fig. 3 shows isosurfaces of the probability densities $|\phi(\mathbf{r})|^2$ of the electron ground state, $e_0$, and the first two excited single-particle states $e_1$ and $e_2$. The light and dark isosurfaces correspond to 10% and 50% of the respective maximum values. The data are displayed for a top-view/along the $c$-axis. The gray shaded area indicates the dot geometry and the dashed lines give the dot barrier interface. The data for the hole ground state, $h_0$, and the first two excited states, $h_1$ and $h_2$, are depicted in the upper row of Fig. 4. The corresponding single-particle energies, also given in the respective figures, for electrons and holes are denoted by $E_{e/h}^i$. Additionally, the figures display the orbital contributions for each TB single-particle state in a table below the charge densities. The calculations include, strain and built-in field effects as well as spin-orbit coupling (SOC) effects; each state is thus two-fold Kramers degenerate. [38]

Turning in a first step to the orbital character of the different single particle states, we observe that all electron states, cf. Fig. 3, are dominated by $s$-orbital ($\geq$ 94%) contributions, consistent for instance with previous $\mathbf{k}\cdot\mathbf{p}$ results. [39, 12] For the holes, cf. Fig. 4, mainly $p_x$- and $p_y$-orbitals contribute to the formation of their single-particle states. The absence of a significant $p_z$ contribution is explained by the following. First, the crystal-field splitting in a WZ crystal breaks the symmetry between $|p_x\rangle$, $|p_y\rangle$ and $|p_z\rangle$-like basis states. In WZ InN and GaN, the $|p_z\rangle$-like state is shifted to a lower energy when compared to $|p_x\rangle$ and $|p_y\rangle$-like states. Furthermore, when looking at the effective masses of the corresponding bands in a bulk system, the crystal field split-off band, mainly formed by $|p_z\rangle$-like states in the absence of SOC, exhibits a lower effective mass when compared to the topmost $|p_x\rangle$- and $|p_y\rangle$-like bulk bands along the WZ $c$-axis. Thus, in case of strong quantum confinement along this axis, as in the case of our 3 nm high $c$-plane $In_{0.2}Ga_{0.8}N$/GaN QD, contributions from the $|p_z\rangle$-like basis states are suppressed in the energetically lowest lying hole states. This explains our observed orbital contributions for the hole states. Furthermore, given the symmetry of the dot geometry and the WZ $c$-plane, the calculated hole states have almost identical $p_x$ and $p_y$ orbital contributions. In general, the observed symmetries of the wave functions as well as the orbital contributions are consistent with previous continuum-based calculations, [39] again showing that our theoretical framework captures accurately the $C_{3v}$-symmetry of the system.

In addition to the orbital character of the different

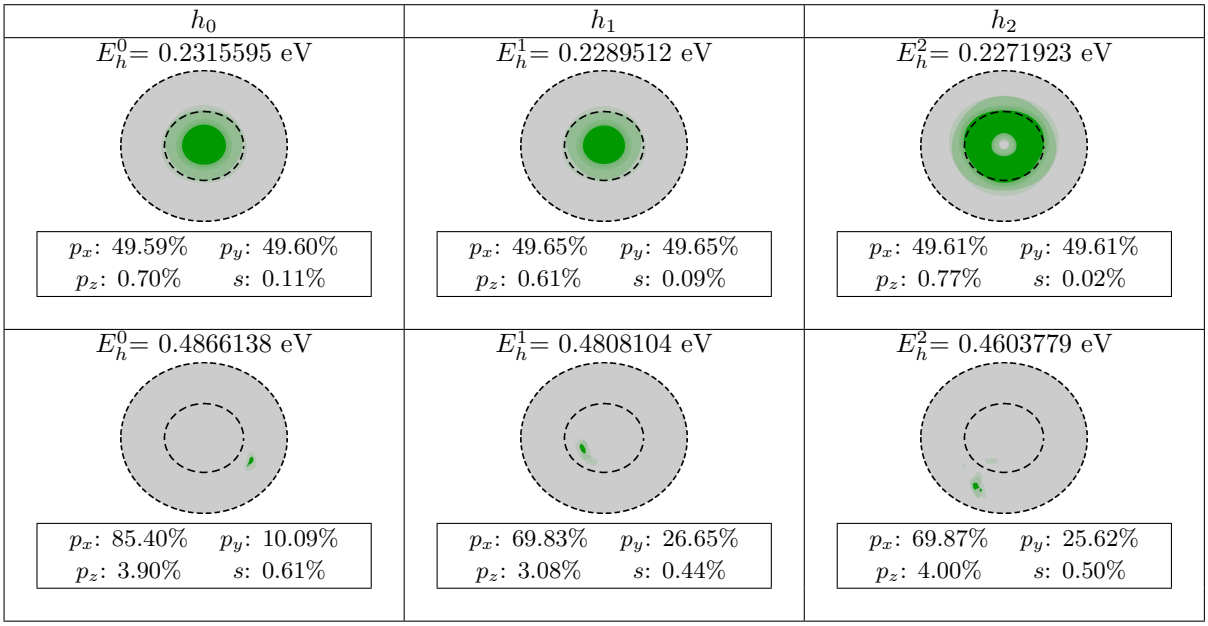



**Figure 4.** Isosurface plots of the single-particle charge densities of the energetically lowest three hole states ($h_0$: ground state; $h_1$: first excited state; $h_2$: second excited state) of a $c$-plane $In_{0.20}Ga_{0.80}N$/GaN QD. The light (dark) green isosurface corresponds to 10% (50%) of the respective maximum charge densities. The different sub-figures give also the single-particles energies $E_h^i$ and the ($s$, $p_x$, $p_y$, $p_z$) orbital contributions (in percent). Upper row: Results for a virtual crystal approximation. Lower row: Same as in the upper row but when random alloy fluctuations are described on an atomistic level. All calculations include strain and built-in field effects as well as spin-orbit coupling. Each single particle state is two-fold Kramers degenerate.

states, the single-particle states depicted in Fig. 3 and 4 can also be classified according to how they transform under the symmetry operations of the point group $C_{3v}$. [15] Classifying the states according to the IRRs of the corresponding point group is very helpful for analyzing the excitonic fine structure. It has been shown and discussed by Baer *et al.* [15] that the electron ground state is invariant under a rotation by $\frac{2\pi}{3}$ around the WZ $c$-axis, whereas the states $e_1$ and $e_2$ transform as $x$- and $y$-like states under the symmetry operations of the $C_{3v}$ group. Therefore, the electron ground state can be denoted as an $s$-like state, while the excited states $e_1$ and $e_2$ are $p$-like states ($p_\pm$-like states). [40] Using the same analysis for the hole states, ground and first excited hole state, $h_0$ and $h_1$, can be classified as $p$-like states, while $h_2$ is $s$-like. [15, 40]

We note that our calculations show only twofold (Kramer's) degenerate states for electrons *and* holes. As discussed already in Ref. [40], the $C_{3v}$ *single* group (no SOC) contains two dimensional IRRs. Therefore, in such a case and when neglecting spin degeneracies, two-fold degenerate states in the energy spectrum (four-fold when including spin) can be expected and are also found in previous studies for instance for the first two excited electron states. [41, 38] We stress that this is in contrast to [001]-oriented InGaAs/GaAs systems, [42] and that in an WZ QD system that preserves the $C_{3v}$ symmetry, strain and built-in fields do *not* lift degeneracies of the electron $p$-states. [36] This aspect can for instance be used to test the impact of boundary conditions on the electronic structure and that these do not lead to artifacts in the calculations. We point out that our calculations in the absence of SOC effects (not shown, but discussed in detail in Ref. [36]) confirm a vanishing electron $p$-state splitting. When including SOC effects, the symmetry of the system is described by the *double* group $\bar{C}_{3v}$. This group contains only two-dimensional IRRs. Thus only two-fold degenerate states are expected and the degeneracy stems from time-reversal symmetry (Kramer's degeneracy). This behavior is indeed found in our VCA calculations, as shown in Figs. 3 and 4. For the hole $p$-state splitting, $\Delta E_{h,p} = E_h^0 - E_h^1$, we find a value of $\Delta E_{h,p} = 2.6$ meV, cf. Fig. 4, while for the electrons the $p$-state splitting $\Delta E_{e,p} = E_e^2 - E_e^1$ is very small with a value of 10.6 $\mu$eV, cf. Fig. 3. Again, in the absence of SOC, $\Delta E_{e,p} = \Delta E_{e,p} = 0$ (not shown). We attribute the small splitting $\Delta E_{e,p}$ between the electron $p$-states, when compared to the hole state splitting $\Delta E_{h,p}$, to the general very small SOC energy in InN and GaN and to the relatively weak conduction band-valence band coupling due to the large band gap. [43]

Overall, several important aspects should be noted. Firstly, in [001]-oriented InGaAs/GaAs QDs, the lifting of the degeneracies of the electron states is often used as a first indicator for a non-vanishing FSS. [44, 13] The fact that for instance the electron $p$-

state splitting is absent in the absence of the SOC and only very small when including SOC, indicates already that a different excitonic fine structure can be expected in *c*-plane InGaN/GaN QDs. Thus, results/knowledge from [001]-oriented InGaAs/GaAs QDs cannot be directly carried over to explain the electronic structure or optical properties of *c*-plane InGaN/GaN dots, as sometimes found in the literature. [45] Secondly, given that the wave functions and the degeneracies of the different levels are consistent with group theoretical arguments as it has to be the case, no artifacts in the electronic structure calculations are introduced by the cubic supercell boundaries. This is very important since this ensures also that the calculation of the (small) excitonic FSS should not be affected by the boundary conditions.

In the next step, we address the question how properties change when treating the InGaN/GaN dot, with nominally the same In content, in a fully atomistic framework, thus accounting for alloy fluctuations on a microscopic level. The results of this analysis are presented in the following section.

*4.1.2. Random alloy fluctuations* In this section we present the single-particle states and energies of the *c*-plane $In_{0.2}Ga_{0.8}N$/GaN QD when accounting for random alloy fluctuations within the dot. In order to study the impact of the alloy microstructure on the results, the calculations have been performed for five different random alloy configurations.

The lower row of Fig. 3 and 4 depict a top-view of the isosurfaces of the ground and the first two excited electron and hole state charge densities in the presence of random alloy fluctuations. Following the VCA description from above, the respective energies and orbital contributions are also given in the figures. The charge densities are displayed for an arbitrary chosen configuration, here configuration 3 (Config.-3). The light and dark isosurfaces correspond to 10% and 50% of the respective maximum values, as in the VCA case.

Comparing the here presented states with the corresponding VCA results (upper row), for both electrons and holes, the charge densities are clearly deformed due to the presence of alloy fluctuations in the dot. Even though the electron charge densities are affected by the local fluctuations, in terms of their nodal structure these densities still, especially for the excited states $e_1$ and $e_2$, resemble to a first approximation $p_x$- or $p_y$-like states. However, for the holes such a classification, based on the nodal structure, is basically impossible. Also, due to higher effective mass of holes when compared to electrons, the holes localize in a smaller region as compared to electrons. Therefore, while the localization characteristics of the electrons, at least to a first approximation are determined by the QD geometry and size, for the holes alloy fluctuations within the dot lead to "extra" localization centers. In general, our results indicate that although random alloy fluctuations perturb the electron wave functions, they have a more dramatic effect on the hole wave functions. We note that similar effects have been observed by different groups in quantum wells. [46, 47, 48]

Overall, given the strong perturbation of the charge densities by the alloy fluctuations, the symmetry of the system is no longer $C_{3v}$ but rather $C_1$. [49] The latter symmetry means that only a rotation of 360° around the WZ *c*-axis is a symmetry operation of the system. The $C_1$ single-point group contains only the IRR $A$ and the double group IRR $A_{1/2}$ [49]. Both of these IRRs are 1-D; from this analysis we can already expect a lifting of any degeneracy in the energy spectrum of our dot system in the presence of alloy fluctuations. We will come back to this and the consequences this has for the excitonic fine structure in the following section.

We note also that the hole states do not necessarily localize directly underneath the electron wave functions. This will obviously affect the electron-hole wave function overlap and therefore further increase the radiative lifetime $\tau$ in the system as discussed in InGaN/GaN quantum wells already. [50, 51] This may also have an impact on the entangled photon emission from *c*-plane InGaN/GaN QDs, given that for the entangled state described in Eq. (2), the product of radiative lifetime $\tau$ and FSS $\Delta_{\mathrm{FSS}}$ needs to be sufficiently small. We will revisit this question when discussing the exciton fine structure and the light polarization characteristics of the emitted photons in more detail.

In a final step, we discuss the orbital character of electron and hole states of the alloy configuration (Config.-3) depicted in Figs. 3 and 4. The electron wave functions mainly consist of *s*-orbital contribution with much weaker contributions from $p_x$-, $p_y$- and $p_z$-orbitals. We observe this for all five different random alloy configurations (not shown). This dominant *s*-orbital contribution in the three energetically lowest electron states is also found in the VCA results. Turning to the hole states, Fig. 4 reveals for the here investigated alloy configuration, that the $p_x$-orbital contribution dominates these states. For other configurations $p_y$-orbital contribution dominates (not shown). This means that in contrast to the VCA-case, where equal contributions of $p_x$ and $p_y$-orbitals are observed in the first three bound states, alloy fluctuations break this symmetry.

Two consequences can now be expected from

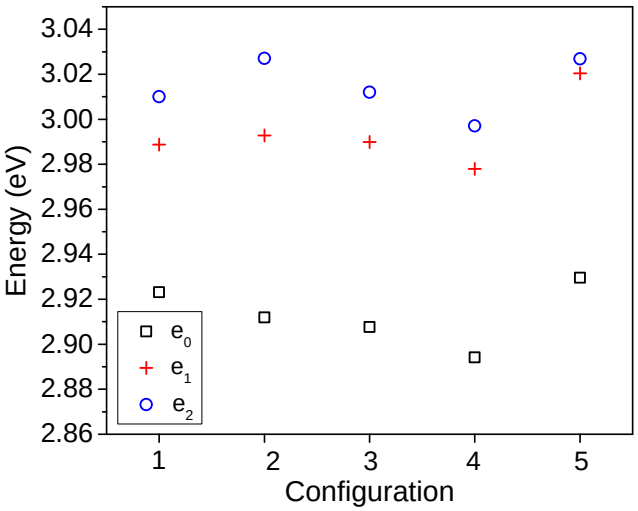



**Figure 5.** Energies of electron ground, $e_0$, first, $e_1$, and second, $e_2$, excited state as a function of the microscopic alloy configurations number.

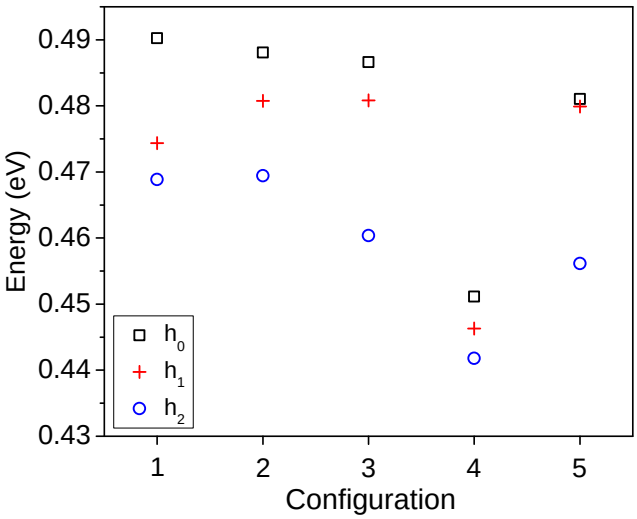



**Figure 6.** Hole ground, $h_0$, first $h_1$ and second $h_2$ excited state energies as a function of the microscopic alloy configurations number.

the observation that alloy fluctuations (i) significantly affect the carrier localization within the dot and (ii) break the symmetry between $p_x$ and $p_y$-orbitals. Turning to (ii) first, it is important to note that the orbital character determines to a large extent the light polarization characteristics of the emitted photons. Thus significant differences between the VCA and the random alloy case can be expected in terms of the light polarization characteristics of emitted photons. We will come back to this aspect when discussing the calculated optical spectra. Secondly, given the strong impact of the alloy fluctuations on the charge densities, it is also expected that the single-particle energies are strongly dependent on the alloy microstructure. For alloy configuration 3, the electron $E_e^i$ and hole $E_h^i$ energies for ground and excited states are given in Fig. 3 and Fig. 4, respectively. Turning to the electron energies first, we find a very large energetic separation between states $e_1$ and $e_2$ ($p$-states) of $\Delta E_e^{\mathrm{p,RA}} \approx 22$ meV. We note that in the VCA calculation, the electron $p$-state splitting was very small, $\Delta E_e^{\mathrm{p,VCA}} = 10.6$ $\mu$eV and originated from SOC effects. As discussed already above, in InGaAs/GaAs QDs, the electron $p$-state splitting has often been used as a first indicator how strongly alloy or even dot shape anisotropies affect the FSS. [44] To study in more detail the impact of the alloy microstructure on the electronic structure, Fig. 5 depicts the energy eigenvalues of the first three bound electron states ($e_0$, $e_1$, $e_2$) as a function of the alloy configuration number. As shown in Fig. 5, the above found large $p$-state splitting in configuration 3 (Config. 3) is not an outlier; the remaining four configurations produce very similar values for the $p$-state splitting $\Delta E_e^{\mathrm{p,RA}}$; $\Delta E_e^{\mathrm{p,RA}}$ varies between $\approx 6 - 34$ meV depending on the alloy microstructure.

Turning to the hole state energies $E_h^i$, data in Fig. 4 for alloy configuration 3 (Config. 3) reveals that the first two hole states $h_0$ and $h_1$, which in the VCA case are classified as $p$-like states, are split by $\Delta E_h^{\mathrm{p,RA}} \approx 6$ meV; in the VCA case we find $\Delta E_h^{\mathrm{p,VCA}} = 2.6$ meV. However, and as already discussed above, while in the case of the electrons one may still want to classify states according to their nodal structure as $s$- or $p$-like, for the holes this classification is not possible. Therefore, it is slightly more complicated to compare the splittings between states directly. Nevertheless, in the following we use the notation $\Delta E_h^{\mathrm{p,RA}}$ to display the difference between the first two hole states $h_0$ and $h_1$. Figure 6 shows that $\Delta E_h^{\mathrm{p,RA}}$ significantly depends on the alloy microstructure; we find that $\Delta E_h^{\mathrm{p,RA}}$ varies between $\approx 1 - 15$ meV.

Overall, our calculations reveal that alloy fluctuations significantly affect the electronic structure of $c$-plane InGaN/GaN QDs. Our data also indicate that the symmetry of the system and as a result, the symmetry of the wave functions is strongly affected. This leads therefore to the question of how the excitonic fine structure is impacted by random alloy fluctuations. Understanding the excitonic fine structure will allow us to understand the impact of alloy fluctuations on entangled photon emission from $c$-plane InGaN/GaN QDs. However, before turning to this question, we study the excitonic fine structure and its consequences for entangled photon emission in VCA.

### *4.2. Excitonic fine structure splitting, excitonic binding energies and light polarization characteristics*

Having discussed the electronic structure of $c$-plane InGaN/GaN QDs in detail above, we focus our attention now on the optical properties. Here, we look at the exciton fine structure, the exciton binding energies, and the expected light polarization characteristics of photons emitted from a $c$-plane InGaN/GaN QD. All these quantities are important to understand when evaluating the potential of $c$-plane InGaN/GaN QDs for entangled photon emission at elevated temperatures. We start our analysis with the VCA description. This will serve as a reference frame for the calculations including random alloy fluctuations, discussed in Sec. 4.2.2.

*4.2.1. Virtual crystal approximation results* In this section we discuss the optical properties of a $c$-plane InGaN/GaN QD described within VCA. But, before looking at the results from such a calculation, we apply group theory to gain insight into the exciton fine structure and polarization characteristics of the emitted photons. Overall, the group theoretical analysis of the VCA data presents also a rigorous benchmark of the theoretical framework.

Even though SOC effects are taken into account in our study, it is informative to start with a discussion where this relatively small contribution is neglected. In the case of a VCA and for the chosen dot geometry the symmetry of the system is $C_{3v}$, as already discussed in detail above. When neglecting SOC effects, the orbital and spin part of a wave function can be decoupled and treated independently. For the considered ideal $c$-plane WZ QD with $C_{3v}$ symmetry, the electron ground state $e_0$ transforms like an $s$-like state (see above) and corresponds to the IRR $A_1$ of the $C_{3v}$ single group. [12, 15] The $p$-like hole ground state $h_0$ can be classified by the IRR $E$. [12, 15] It is important to note that $E$ is a two-dimensional (2-D) IRR. Thus in the absence of SOC, the hole ground state is two-fold degenerate (four-fold when including spin), as for instance also found in the calculations of Ref. [38].

Focussing on the orbital part of the states involved in $e_0$-$h_0$ transitions, the corresponding exciton states transform as $A_1 \otimes E = E$. This means, the exciton ground state is two-fold degenerate since $E$ is a 2-D IRR. Taking now electron and hole spins into account, the resulting states are either singlet or triplet states. [36] Combining orbital and spin parts of the excitonic wave function, and neglecting initially also electron-hole exchange terms, the exciton ground state is eight-fold degenerate. The electron-hole exchange interaction lifts this degeneracy and one is left with a two-fold degenerate state stemming from $E$ symmetry of the orbital part and the 1-D $D_0$ IRR of the spin part and a six-fold degenerate state stemming from $E$ symmetry of the orbital part and the 3-D $D_1$ IRR of the spin part.

Taking SOC effects into account, as done in our VCA calculations, the single particle states transform according to the IRRs of the $C_{3v}$ *double* group. As discussed above, the hole ground state $h_0$ has $p_x$- and $p_y$-like character and transforms according to the 2-D $E_{3/2}$ representation. The electron ground state $e_0$ has $s$-like character and transforms as the two-dimensional IRR $E_{1/2}$. The exciton ground states transform according to $E_{1/2} \otimes E_{3/2} = E \oplus E$. Since $E$ is a 2-D IRR of the $C_{3v}$ group, two two-fold degenerate excitonic states are expected. Additionally, following Ref. [12, 49], the two doublets are formed by bright states and the excitonic emission spectrum is polarized in the $(x, y)$ plane, thus perpendicular to $c$-axis ($z$-axis). In the presence of electron-hole exchange interaction, the degeneracy of the two bright $E$-symmetric states is lifted. We denote the splitting between these two pairs of $E$-symmetric bright states as the (bright-bright) FSS. We stress that the splitting between the bright states within a $E$-symmetric doublet is zero. It is important to note that this exciton fine structure is very different from a $C_{2v}$-symmetric dot, e.g. an InGaAs/GaAs QD grown along the [001]-direction of the ZB lattice. In a $C_{2v}$-symmetric system the four lowest excitonic states consist of a dark state, a state where the emitted photon is polarized along the QD growth direction (e.g. [001]-direction) and two bright states, which emit photons polarized within the growth plane ($x-y$-plane). The FSS of [001]-oriented InGaAs/GaAs dots usually quoted in the literature, is the splitting between the bright excitonic ground states. The magnitude of this (bright-bright) splitting, along with the radiative recombination lifetime determines the ability of a given dot to emit entangled photon pairs, see Eqs. (1) and (2). The comparison between the excitonic fine structures in $C_{3v}$ and $C_{2v}$ symmetric dots highlights now again very clearly the benefit of targeting $C_{3v}$ symmetric dot systems: in this case one is left with two doublets of bright exciton states which all emit circularly polarized light. Therefore, $c$-plane III-N systems should *in principle* be ideal candidates for polarization entangled photon pairs.

Equipped with all this knowledge, we now present the outcome of our VCA calculations for $c$-plane InGaN/GaN QDs. To compare the calculated VCA FSS values with results from the fully atomistic treatment (including alloy fluctuations), we proceed as follows: the energies of the four energetically lowest lying exciton states, $E_X^i$, are always plotted with respect to the ground state energy, $E_X^{\mathrm{GS}}$ ($E_X^0$) so that we are left with $\Delta E_X^i = E_X^i - E_X^{\mathrm{GS}}$, where

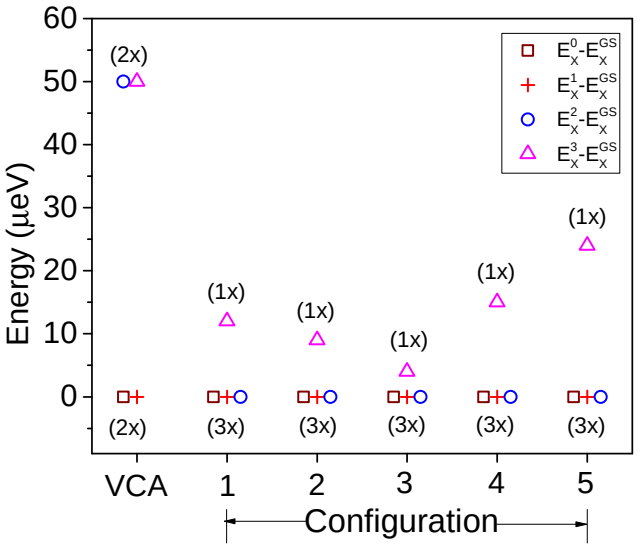



**Figure 7.** Fine structure splitting of the four energetically lowest exciton states in a $c$-plane $In_{0.2}Ga_{0.8}N$/GaN QD. The data are shown for a virtual crystal approximation (VCA) of the dot and when considering five different (random) alloy configurations. The data is always displayed with respect to the exciton ground state energy ($E_X^{GS} = E_X^0$).

$i \in \{0, 1, 2, 3\}$. The degeneracy of each level is indicated by $N$x, were $N$ gives the degeneracy (e.g. 2x=two-fold degenerate exciton state). The ground and the first three excited states are denoted by square, cross, circle and triangle symbols, respectively. Figure 7 depicts $\Delta E_X^i$ for the VCA-case and the random configurations, which will be discussed later. Looking at the VCA data, our calculations show the group theoretically predicted behavior of two sets of two-fold degenerate exciton states. These levels are split by a (bright) FSS of $\Delta_{\text{FSS}} \approx 50$ μeV. We note that when neglecting the electron-hole exchange interaction in the calculations (thus only direct Coulomb terms are included) a four-fold degenerate exciton ground state is found (not shown), inline with our group theoretical analysis. Thus, the electron-hole exchange interaction is responsible for the observed FSS. Moreover, it is important to note that even though the SOC effect is weak in InN and GaN systems, at least when compared to InAs or GaAs systems, [52, 43] without the SOC excitonic fine structure looks completely different as discussed above in detail.

Having discussed excitonic fine structure we turn in a second step to the light polarization characteristics of photons emitted/absoped by the considered dots. To do so, we study the excitonic absorption and emission spectra of the $c$-plane InGaN QD and compare the calculated spectra with the group theoretical predictions. Figure 8 (a) shows a polar plot of the optical intensity of the exciton ground state emission. Here we have varied the light polarization vector within the $x-y$-plane and the figure reveals circularly polarized light, consistent with the group theoretical analysis above; this behavior is ideally suited for polarization entangled photon emission, see Eq. (1). To shed further light onto the optical properties of such a $C_{3v}$-symmetric dot, Fig. 8 (b) displays the excitonic absorption spectrum for two orthogonal light polarization vectors. Using the polar plot from Fig. 8 (a), the $x$-polarized light corresponds to an angle of 0°, while $y$-polarized light corresponds to an angle of 90°. Figure 8 (b) reveals, independent of the light polarization, two distinct absorption lines are separated by 50 $\mu$eV. Note that the $x$- and $y$-polarized absorption are overlapping and thus can not be distinguished. The splitting between the two absorption peaks is inline with the excitonic fine structure discussed above and shown in Fig. 7. Overall, the results are in accordance with the group theoretical prediction that (i) the doublets present in the excitonic fine structure are bright and (ii) the emitted light is polarized in the $(x-y)$ plane. Therefore, photons emitted via these transitions can be classified as $(\sigma^-)$ or right $(\sigma^+)$ circularly polarized.

We stress again, that the FSS of $\Delta_{\text{FSS}} = 50$ μeV between bright excitonic doublets is of secondary importance for entangled photon emission. This stems from the fact that the FSS of the two bright states per doublet is zero and the light emitted is circularly polarized. As a result, in the XX-X exciton cascade involving these bright doublet states, one is left with the situation schematically depicted in Fig. 1 (a) where due to the degeneracies of the bright exciton ground states, both left and right arms of the cascade emit circularly polarized light. Therefore, a polarization entangled state given by Eq. (1) can be obtained. We highlight again that all this originates from the underlying $C_{3v}$-symmetry of the system, so that this analysis is also applicable to other system ($c$-plane GaN/AlN; [111]-oriented InAs/GaAs QDs) which exhibits and preserves a $C_{3v}$ symmetry.

While all these aspects already highlight the benefit of a $C_{3v}$ symmetric dot for polarization entangled photon emission, WZ III-N $c$-plane dots should ideally offer, in part thanks to the large band offsets, excitonic binding energies higher than the thermal energy at room temperature. Thus, in that case polarization entangled photon emission at much higher temperatures as in the arsenide systems can be achieved. Thus, we have also analyzed the excitonic binding energy $E_X^b$ of the considered $c$-plane $In_{0.2}Ga_{0.8}N$/GaN dot. The exciton binding energy is calculated via $E_X^b = (E_e^0 - E_h^0 - E_X)$, where $E_e^0$ and $E_h^0$ are the electron and hole single-particle ground state energies, respectively, while $E_X$ is the exciton ground state energy. Figure 9 depicts $E_X^b$ for the VCA case

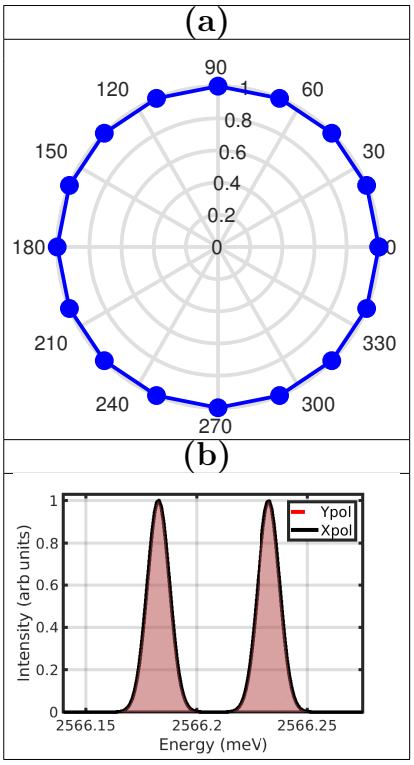



**Figure 8.** (a) Polar plot of the optical intensity in the $c$-plane ($x-y$-plane) for the excitonic ground state emission of a $c$-plane $In_{0.2}Ga_{0.8}N$/GaN QD when treated in a virtual crystal approximation. (b) Excitonic absorption spectrum for two orthogonal light polarization vectors. The light polarization vector along the $x$-axis ($y$-axis) corresponds to 0° (90°) in the polar plot of (a). Note that the $x$- and $y$-polarized absorption are overlapping and thus can not be distinguished.

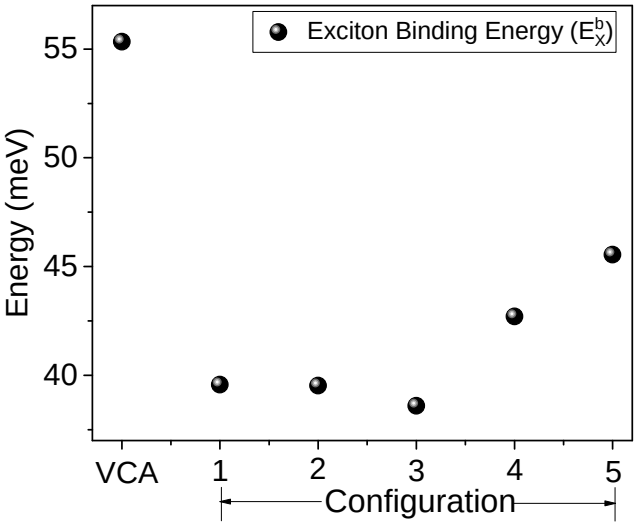



**Figure 9.** Excitonic binding energy $E_X^b$ of $c$-plane $In_{0.2}Ga_{0.8}N$/GaN QDs. The data are shown for the virtual crystal approximation (VCA) case and for the five different random alloy configurations.

and the five different random alloy configurations. For the VCA case we obtain a very large exciton binding energy of ≈ 55 meV, which clearly exceeds the thermal energy at room temperature of ≈ 25 meV. Overall, and taking the large excitonic binding energy, excitonic fine structure and the light polarization characteristics of the emitted photons into account, our study shows that $c$-plane InGaN QDs are in principle ideal candidates for entangled photon emission at elevated temperatures.

Having discussed the *ideal* VCA case we turn now and focus our attention on the impact of random alloy fluctuations on the optical properties of $c$-plane InGaN/GaN QDs. As above, special attention will be paid to impact of such alloy fluctuations on entangled photon emission from such dots.

*4.2.2. Random alloy fluctuation results* We address in this section the consequences of random alloy fluctuations in $c$-plane InGaN/GaN QDs on their ability to emit polarization entangled photon pairs. Before presenting the results of our CI calculations, similarly to the VCA case, we start with a group theoretical analysis.

Building on our discussion of the single-particle states in Sec. 4.1.2, we have seen that the $C_{3v}$-symmetry is lost in the presence of random alloy fluctuations. As we have already mentioned in Sec. 4.1.2, we are left with a $C_1$ symmetry. Again neglecting initially the weak SOC, the electron $e_0$ and hole $h_0$ ground states transform according to the IRR $A$ of the $C_1$ single group. Thus the exciton state related to the $e_0$-$h_0$ transition has $A \otimes A = A$ symmetry, which is 1-D IRR. When including spin, but neglecting SOC and electron-hole interaction in the description, the exciton ground state is four-fold degenerate. The electron-hole exchange interaction splits this four-fold degenerate state into singlet and triplet states. Accounting for SOC, electron and hole ground states transform according to the $A_{1/2}$ IRR of the $C_1$ double group. In this case, the excitonic states transform according to $A_{1/2} \otimes A_{1/2} = A$. Since $A$ is a 1-D IRR, one expects four non-degenerate states for the four energetically lowest exciton states.

Figure 7 shows the exciton fine structure for the five different random alloy configurations. From this figure one can infer that when taking random alloy fluctuations into account the excitonic FSS is very different from the VCA case. While in VCA one observes two doublets of degenerate states, in the random alloy case we find a non-degenerate state and an (approximately) three-fold degenerate exciton state; this finding is independent of the configuration number, thus the alloy microstructure. Overall, bearing in mind our group theoretical analysis: for a system with $C_1$-symmetry, including SOC and electron-hole exchange interaction, the energetically

lowest lying excitonic states are expected to be non-degenerate. Here, our calculated excitonic fine structure is similar to the case expected in the absence of SOC effects, where due to electron-hole exchange interaction a singlet (non-degenerate) state and a triplet (three-fold degenerate) state is expected. While one might be tempted to classify the calculated excitonic states as being singlet and triplet states, we note that the three states forming the "triplet" states are only approximately degenerate, indicating that SOC starts to mix singlet and triplet states as observed in other systems. [53] The small FSS between "singlet" and "triplet" states of 5-25 $\mu$eV can facilitate such a mixing. The small FSS calculated in our $c$-plane system is attributed to the presence of the strong electrostatic built-in field ($\approx$ 0.09 MV/cm) [54] in $c$-plane InGaN/GaN QDs along the $c$-axis. This field spatially separates electron and hole wave functions along the growth direction of the dot and reduces therefore the electron-hole exchange Coulomb matrix elements in comparison to system where such a strong field is absent, e.g. [001]-oriented InGaAs/GaAs dots. Therefore, the combination of SOC and small electron-hole exchange interaction may lead to singlet-triplet state mixing. Before looking at light polarization characteristics and how this quantity is affected by random alloy fluctuations we first discuss the exciton binding energies. As shown in Fig. 9, and similar to the VCA case, we observed large excitonic binding energy values ranging between 38-46 meV. Therefore, excitons in these systems are expected to be stable near room temperature irrespective of the alloy microstructure, since $E_X^b$ still exceeds the thermal energy at room temperature.

Having discussed the excitonic fine structure and the exciton binding energies, we target now the light polarization characteristic of the emitted photons. As highlighted already above, not only the FSS is important but also circularly or orthogonally polarized photons are required to achieve polarization entangled photon pairs. In the following we use the random alloy configuration 5 (Config. 5) as an example, since it exhibits the largest FSS (cf. Fig. 7). We note here that all results discussed below for this selected configuration reflect the behavior found in the four remaining alloy configurations.

Figure 10 (a) depicts a polar plot of the optical intensity of the exciton ground state emission for Config. 5. The angle dependence of optical intensity is again analyzed within the $c$-plane. Comparing this result with the data from the VCA calculation, Fig. 8, the difference is striking. While in the VCA case one is left with circularly polarized light, in the random alloy cases the light is linearly polarized. We note that we find strongly linearly polarized light for all

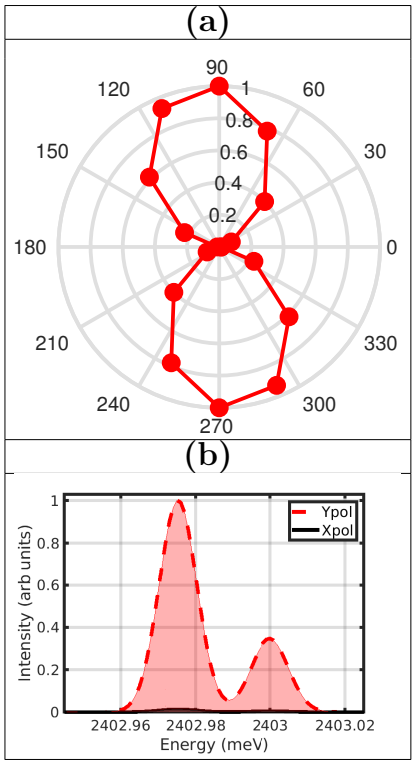



**Figure 10.** (a) Polar plot of the optical intensity in the $c$-plane ($x-y$-plane) of the excitonic ground state emission of a $c$-plane $In_{0.2}Ga_{0.8}N$/GaN QD when accounting for random alloy fluctuations. (b) Excitonic absorption spectrum for two orthogonal light polarization vectors. The light polarization vector along the $x$-axis ($y$-axis) corresponds to 0° (90°) in the polar plot displayed in (a).

other random alloy configurations. As discussed above, linearly polarized light emission and a non vanishing FSS is not necessarily a problem for entangled photon emission as long as (i) the FSS is not larger than the linewidth, (ii) the radiative lifetime is small and (iii) orthogonally polarized photon emission is possible from the XX-X cascade. To shed light onto aspect (iii), Fig. 10 (b) displays the excitonic absorption spectra for Config. 5. The absorption spectra reveals two peaks, which are basically separated by the FSS found for Config. 5 (cf. Fig. 7), thus reflecting the excitonic fine structure discussed above. We note also that if the calculated states were triplet and singlet states, transitions involving the triplet states should have been dark. However, as Fig. 10 (b) reveals this is not the case. Therefore, we conclude that the small electron and hole exchange interaction in conjunction with the presence of the SOC leads to a singlet and triplet state mixing. As a consequence the energetically lowest four excitonic states are all bright. At first glance, the fact that all four excitonic states are bright and that the FSS is relatively small may still be compatible with generating entangled photon pairs.

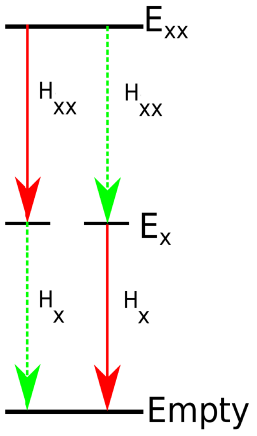



**Figure 11.** Schematic illustration of the light polarization properties of the emitted photons from biexciton-exciton cascade in a *c*-plane InGaN/GaN QD when including random alloy fluctuations. Only two states from the three-fold degenerate states are selected. The emitted photons are horizontally polarized to a given reference axis.

The light polarization characteristics, however, are a major drawback for *polarization* entangled photon emission in the case of random alloy fluctuations. Looking back at aspect (iii), emission of orthogonally polarized photons is required to generate such a photon pair. But as Fig. 10 (b) reveals, photons generated from transitions involving the different bright excitonic states have the same polarization characteristics; the situation is schematically illustrated in in Fig. 11. Using the notation from Fig. 11, only states of the form

$$|\psi\rangle = \frac{1}{\sqrt{2}}\left(|H_{XX}H_X\rangle + |H_{XX}H_X\rangle\right) \quad (3)$$

can be realized. Such a state is *not* a polarization entangled state. Therefore, even though we have a three-fold degenerate bright excitonic state (vanishing FSS), the polarization characteristics of the emitted photons will prohibit polarization entanglement, in the case that the dot exhibits random alloy fluctuations.

The (in-plane) light polarization characteristics of excitonic transitions in *c*-plane InGaN/GaN QDs has also been studied experimentally. [55, 56, 57] Amloy *et al.* [55] for instance reports strongly linearly polarized excitonic emission spectra from single *c*-plane InGaN/GaN QDs with 20% In content. In Refs. [56, 57] also strongly linearly polarized excitonic transitions from InGaN/GaN QDs have been reported. Overall, these findings are inline with the here reported theoretical results.

## 5. Conclusion

In this study we have analyzed the potential of *c*-plane InGaN/GaN dots for polarization entangled photon emission at elevated temperatures. Special attention was paid to consequences of random alloy fluctuations for this question. The analysis was carried out in a fully atomistic many body framework accompanied by group theoretical considerations.

Using virtual crystal approximation calculations as a starting point, thus neglecting alloy fluctuations entirely, we find an excitonic fine structure that is very different from the fine structure in more conventional III-V-based quantum dot systems but ideally suited for entangled photon emission. Also the polarization characteristics of the emitted photons meet the requirements for polarization entanglement. Additionally, our analysis reveals a very large excitonic binding energy (≈50 meV). This large binding energy exceeds the thermal energy at room temperature and should thus support stable excitons near room temperature. Overall, our studies on these *idealized* structures indicate that *c*-plane InGaN/GaN quantum dots are highly attractive for high temperature entangled photon emission.

While the benefit of large excitonic binding energies is still preserved when accounting for random alloy fluctuations on a microscopic level, the excitonic fine structure is significantly modified when compared to the virtual crystal approximation. Our calculations show that a major drawback of this modified fine structure stems from the fact that while energetically lowest excitonic states are all bright and degenerate, the photons emitted from a biexciton-exciton cascade involving these states exhibit basically the same polarization characteristics. This aspect thus prevents polarization entangled photon emission via the biexciton-exciton cascade in *c*-plane InGaN/GaN quantum dots.

We note that our underlying assumption is a random alloy description of the quantum dot microstructure. If the alloy composition can be manipulated, for instance by introducing In atom clustering as for instance observed in non-polar InGaN systems, [58] there may be ways to tailor the alloy microstructure so that the system exhibits again a $C_{3v}$ symmetry. In doing so the full potential of *c*-plane InGaN/GaN dots may be exploited for polarization entangled photon pairs.

Going beyond polarization entanglement, photon entanglement may be realized by using other approaches such as the arrival time of a single photon [59]. Time-binned entangled photon pairs have been realized recently by employing coherent superposition of "early" and "late" photons in a biexciton-exciton cascade; [59] this scheme does not rely on the polarization characteristics of the emitted photons. Finally, twin photon emission, where actually photons of the same polarization are required, provide a further avenue for non-classical light emission. [60] All these schemes,

which have mainly been addressed for arsenide-based system, should benefit from the here observed large excitonic binding energies and in general the large band offset. Therefore *c*-plane III-N based QD system should provide interesting properties and routes to achieve non-classical light emission at elevated temperatures over a wide emission wavelength range.

**Acknowledgments**

The authors thank the Science Foundation Ireland (project nos. 13/SIRG/2210, 17/CDA/4789, and 12/RC/2276 P2) for the financial support of this project and Emanuele Pelucchi for fruitful discussions. Furthermore,computing resources provided by Science Foundation Ireland (SFI) to the Tyndall National Institute and Higher Education Authority funded Irish Centre for High End Computing (ICHEC) are acknowledged.

## Appendix

In this section we provide insight into theory underlying the results presented in the main text of the manuscript. We will start with the electronic structure theory applied, Sec. Appendix A. The details of the configuration interaction calculations are given in Sec. Appendix B.

## Appendix A. Electronic structure theory

To gain insight into the electronic structure of *c*-plane InGaN/GaN QDs we have employed a nearest neighbor $sp^3$ model [61]. In general, this model has already been discussed in detail in our previous work, targeting bulk and quantum well structures. For these systems it shows very good agreement with available experimental data for a variety of different aspects. [27, 62, 63, 50, 51] Overall, this model presents now an ideal starting point for calculating the electronic structure of InGaN/GaN QDs on a microscopic level. We discuss in the following how the model is adjusted to describe the electronic structure of QDs and, in a second step, their excitonic fine structure. While the above discussed TB model is intrinsically an atomistic approach, we detail also how it is modified to obtain a VCA model that still keeps the underlying atomistic symmetry. We first start with the fully atomistic approach, Sec. Appendix A.1 before turning to the VCA description, Sec. Appendix A.2.

### *Appendix A.1. Fully atomistic model*

Our nearest neighbor TB model has been parametrized using (Heyd-Scuseria-Ernzerhof) hybrid functional density functional band structure data for GaN and InN. [27] This model gives a very good description of the unstrained bulk band structures near the Γ-point but also at the edges of the first Brillouin zone of lowest conduction and highest valence bands of both InN and GaN. We have extended this parameterization here to include SOC effects. [60] Even though the SOC is small in InN ($\Delta_{\mathrm{SOC}}^{\mathrm{InN}} = 5$ meV) and GaN ($\Delta_{\mathrm{SOC}}^{\mathrm{GaN}} = 17$ meV), at least when compared to InAs ($\Delta_{\mathrm{SOC}}^{\mathrm{InAs}} = 390$ meV) and GaAs ($\Delta_{\mathrm{SOC}}^{\mathrm{GaAs}} = 341$ meV), these effects are important for accurate description of the excitonic fine structure. SOC effects are included in the model by the widely used approach of Chadi [64]. Given the small values of the SOC, the refitted TB parameters when including SOC effects, summarized in Table A1, differ only slightly from those in the absence of SOC. Also, given that we are mainly interested in the SOC splitting of the bands near the Γ-point, we do not distinguish between the anion and cation based SOC TB parameters $\lambda_i$; distinguishing between $\lambda_c$ and $\lambda_a$ would only result in the situation that splittings of states lying energetically far away from the band edges would be modified differently. However, these energetically remote bands are of secondary importance for the direct band gap materials InN and GaN, where bands close to the band edge are mainly relevant for optical properties of InGaN/GaN QDs. To treat alloy effects in this fully atomistic framework, we use for the anion sites composition weighted averages of the TB parameters describing the binary materials; such an approach has also been widely applied by other groups. [65, 66, 67] This averaging procedure is not required for cations, given that their nearest neighbors are always nitrogen atoms. Furthermore, to align the energy scales between InGaN and GaN, we then use natural band offsets from HSE-DFT calculations. [17]

To study heterostructures, also strain effects have

**Table A1.** Tight-binding parameters (in eV) for the nearest neighbor $sp^3$ model of wurtzite InN and GaN with ($\Delta_{\mathrm{so}} \neq 0$) and without ($\Delta_{\mathrm{so}} = 0$) spin-orbit coupling effects. The notation of Ref. [68] is used.

| | $\Delta_{\mathrm{so}} = 0$ | | $\Delta_{\mathrm{so}} \neq 0$ | |
|---|---|---|---|---|
| | InN [eV] | GaN [eV] | InN [eV] | GaN [eV] |
| E(s,a) | -11.9173 | -10.6158 | -11.9173 | -10.6158 |
| E(p,a) | 0.4886 | 0.8183 | 0.4867 | 0.8127 |
| E($p_z$,a) | 0.4558 | 0.7926 | 0.4572 | 0.7849 |
| E(s,c) | 0.4837 | 0.9122 | 0.4837 | 0.9122 |
| E(p,c) | 6.5322 | 6.6788 | 6.5322 | 6.6788 |
| V(s,s) | -1.6124 | -5.9749 | -1.6124 | -5.9749 |
| V(x,x) | 1.7863 | 2.3381 | 1.7863 | 2.3381 |
| V(x,y) | 4.8338 | 5.4697 | 4.8338 | 5.4697 |
| V(sa,pc) | 1.8919 | 4.0909 | 1.8919 | 4.0909 |
| V(pa,sc) | 6.1355 | 8.6655 | 6.1355 | 8.6655 |
| $\lambda_a$ | 0 | 0 | 0.0017 | 0.0052 |
| $\lambda_c$ | 0 | 0 | 0.0017 | 0.0052 |

to be included in the model. To do so, deformation potentials from HSE-DFT calculations [17] have been used and included in the framework via a site-diagonal correction as detailed in Ref. [46]. In doing so the deformation potentials are input parameters and no further fitting is required. To obtain the relaxed atomic positions, we apply here Martin's valence force field (VFF) model, which includes electrostatic interactions in the system explicitly and reproduces characteristics of a real WZ system, for instance, $\frac{c}{a}$ ratios, accurately. [69, 27] More details on the model can be found elsewhere. [46, 27]

Finally, in WZ (local) strain effects will also give rise to very strong (local) piezoelectric polarization fields, which in *c*-plane InGaN/GaN QDs result in strong spatial separation of electrons and holes along the growth direction. In addition, and different to [001]-oriented ZB InGaAs/GaAs, WZ III-N materials exhibit also a spontaneous polarization that is even present in the absence of strain effects. To achieve a microscopic description of these polarization effects, we employ here our recently developed local polarization theory. So far this model has been applied to *QW* systems and care must be taken when employing it in a *QD* situation. In our local polarization theory the $i$th component of the polarization vector field $\mathbf{P}$ can be written as: [27]

$$P_i = \underbrace{\sum_{j=1}^{6} e_{ij}^{(0)} \epsilon_j}_{\text{macroscopic}} + \underbrace{P_i^{\text{sp}} - \frac{e}{V_0} \frac{Z_i^0}{N_{\text{coor}}^0} \left( \mu_i - \sum_{j=1}^{3} \left(\delta_{ij} + \epsilon_{ij}\right) \mu_{j,0} \right)}_{\text{local}} \quad \text{(A.1)}$$

For the local part, Eq. (A.2), that contains the spontaneous polarization $P_i^{\text{sp}}$, the bond asymmetry parameter $\mu$, defined as a summation over the nearest neighbor distances, the asymmetry parameter of the unstrained system $\mu_0$, the strain tensor $\epsilon$, the Born effective charges $Z$, the number of nearest neighbors $N_{\text{coor}}^0$, and the elementary charge $e$, no changes are required to treat a QD instead of a QW. The macroscopic part, Eq. (A.1), that contains the clamped ion contribution, the situation is different. In a QW system, the macroscopic part is zero in the barrier material (e.g. GaN) but nonvanishing and constant in the well (e.g. InGaN). This results from the fact that the barrier is unstrained and in the well the macroscopic strain is constant. However, this does not hold for a QD where the strain field is position dependent and also non-vanishing in the barrier material close to the dot. To take this into account, we apply a surface integral approach to calculate on our atomistic (ideal WZ) grid the strain field from: [26]

$$\epsilon_{ij}(\mathbf{r}) = \delta_{ij}\epsilon_0\chi_{QD} + \frac{\epsilon_0 A}{4\pi} \int_{QD} \frac{(x_i - x_i')}{|\mathbf{r} - \mathbf{r}'|^3} \hat{\mathbf{n}}_j \cdot d\mathbf{S}' \quad \text{(A.2)}$$

where the primed quantities refer to points on the surface of the dot, $(x_1, x_2, x_3) \equiv (x, y, z)$, $\hat{\mathbf{n}}_j$ is the unit vector in the $j$-direction, and $A = (1+\nu)/(1-\nu)$, with $\nu$ being the Poisson ratio. The characteristic function $\chi_{QD}$ is equal to 1 inside the dot and zero outside. The isotropic misfit strain is denoted by $\epsilon_0$ and assumed equal to $\frac{1}{3}(2\epsilon_{0,a} + \epsilon_{0,c})$, where $\epsilon_{0,a}$ is the misfit strain in the *c*-plane, and $\epsilon_{0,c}$ is the misfit strain along the *c*-axis. This analytic model allows us to calculate in a continuum-based frame on our atomistic grid the clamped ion contribution required in the local polarization theory, Eqs. (A.1) and (A.2). Once the local polarization vector field is known we use a point dipole method to calculate the corresponding built-in potential. [27] This (local) built-in potential is included in the TB model as a diagonal correction, which is a widely used ansatz to electrostatic built-in fields in a TB model. [40]

Having discussed the fully atomistic framework to study the electronic structure of InGaN/GaN QDs, and to expose the impact of alloy fluctuations on their electronic structure and finally optical properties, we use a VCA model as a reference system. In the next section we briefly describe how we construct such a model while still keeping the underlying $C_{3v}$ symmetry of the combined system of WZ crystal structure and QD geometry.

### *Appendix A.2. Virtual crystal approximation*

To obtain a VCA-TB description of an alloyed $\text{In}_x\text{Ga}_{1-x}\text{N}$ QD system, the required TB parameters are the composition weighted averages of the InN and GaN binary TB parameters. We note that the chosen approach not necessarily agrees with the band gap bowing parameter obtained from a fully atomistic description, however, the transition energy for our study here is of secondary importance since the VCA-TB model is designed to keep the perfect $C_{3v}$ symmetry of the system. Therefore, we use the VCA-TB parameters and assume an ideal WZ lattice: in the barrier material we use the GaN TB parameters while in the QD region virtual InGaN atoms described by VCA-TB parameters. For a comparison with the fully atomistic approach, an In content of 20% has been assumed. To obtain the strain field in and around the dot, we use the surface integral approach discussed above, Eq. (A.2). This gives an easy and straightforward approach to obtain a VCA compatible strain field that still keeps the $C_{3v}$-symmetry of the system. The additional benefit of Eq. (A.2) is that it

assumes an infinite matrix surround the dot. Therefore the rectangular boundary conditions of the simulation cell are not a problem for this approach.

Finally, to obtain the electrostatic built-in potential, arising from spontaneous and piezoelectric polarization, we also use a surface integral technique. [26] This method is a simple real space model that for certain dot geometries (e.g. cuboid) can give analytic results for polarization potential in and around a dot. This method uses surface integrals to evaluate these values and assumes that the QD is buried in an infinite system; therefore, boundary condition will not play a role. Since this method can be used with any arbitrary underlying grid, this is attractive for use in our TB model. The piezoelectric polarization potential is obtained via:

$$\varphi_{str}(\mathbf{r}) = J\int_{QD}\frac{(x_3-x_3')^2}{|\mathbf{r}-\mathbf{r}'|^3}\hat{\mathbf{n}}_3\cdot d\mathbf{S}' + K\int_{QD}\frac{1}{|\mathbf{r}-\mathbf{r}'|}\hat{\mathbf{n}}_3\cdot d\mathbf{S}' \tag{A.3}$$

with

$$J=\frac{-\epsilon_0 A\,(2e_{15}-e_{33}+e_{31})}{8\pi\varepsilon_r\varepsilon_0}$$

and

$$K=\frac{\epsilon_0}{8\pi\varepsilon_0\varepsilon_r}\left[4e_{31}+2e_{33}-A\,(2e_{15}+e_{31}+e_{33})\right]\ .$$

The piezoelectric coefficients are denoted by $e_{ij}$. The potential due to spontaneous polarization is obtained from

$$\varphi_{spo}(\mathbf{r})=\frac{1}{4\pi\varepsilon_r\varepsilon_0}\left[\int_{QD}\frac{\mathbf{P}_{QD}\cdot d\mathbf{S}'}{|\mathbf{r}-\mathbf{r}'|}+\int_M\frac{\mathbf{P}_M\cdot d\mathbf{S}_M}{|\mathbf{r}-\mathbf{r}_M|}\right]\ .$$

The dielectric constant $\epsilon_r$ and $\mathbf{P}_{QD}$ ($\mathbf{P}_M$) is the constant spontaneous polarization of the dot (barrier) material. To obtain the different relevant material parameters we use a linear interpolation between values of binary materials InN and GaN weighted with the In/Ga content.

We stress again, that such a VCA description with an underlying WZ lattice, using dot geometries of high symmetry (e.g. truncated cones or lens-shaped geometries) and strain and polarization fields from a surface integral approach will result in an ideal $C_{3v}$ symmetric system. Thus, the results from the introduced VCA model presents an ideal reference point to study any symmetry breaking effect of alloy fluctuations treated in the fully atomistic model discussed above. Again, the purpose of the VCA model is *not* to match transition energies; preserving symmetries is the main purpose of our VCA studies.

## Appendix B. Many-body calculations

The theoretical analysis of optical properties of semiconductor QDs is inherently a many body problem. Here, we apply the configuration interaction (CI) scheme to gain insight into the optical properties of $c$-plane InGaN/GaN QDs. In the CI method the many-body Hamiltonian is constructed in the basis of anti-symmetrized products of (bound) single-particle electron and hole states. In general, the many-body Hamiltonian $H_{\rm MB}$ describing a system $N_e$ electrons and $N_h$ holes is given by:

$$\begin{aligned}H_{\rm MB} = &\sum_i E_e^i c_i^\dagger c_i + \sum_\alpha E_h^\alpha h_\alpha^\dagger h_\alpha \\ &+\frac{1}{2}\sum_{ijkl}V_{ijkl}^{ee}c_i^\dagger c_j^\dagger c_k c_l + \frac{1}{2}\sum_{\alpha\beta\gamma\delta}V_{\alpha\beta\gamma\delta}^{hh}h_\alpha^\dagger h_\beta^\dagger h_\gamma h_\delta \\ &-\sum_{il}\sum_{\beta\gamma}\left(V_{i\beta\gamma l}^{eh,di}-V_{i\beta l\gamma}^{eh,ex}\right)c_i^\dagger h_\alpha^\dagger h_\gamma c_l\ .\end{aligned} \tag{B.1}$$

Here, the operator $c_i^\dagger$ ($c_i$) describes/denotes the creation (annihilation) of an electron in the single-particle state $i$; $h_\alpha^\dagger$ ($h_\alpha$) create (annihilate) a hole in the state $\alpha$. The two terms in the first line of Eq. (B.1) accounts for the electron, $E_e^i$, and hole, $E_h^i$, single-particle energies. The terms in line 2 of Eq. (B.1) describe electron-electron and hole-hole repulsive Coulomb interactions; we note that since we are dealing with excitons ($N_e = 1$, $N_h = 1$) in this work, these terms are not relevant here. The last line in Eq. B.1 describes both the direct ($di$) and exchange ($ex$) electron-hole interaction. The single-particle energies $E_e^i$ and $E_h^\alpha$ are obtained from our TB calculations. The Coulomb matrix elements $V^{eh,di}$ and $V^{eh,ex}$ are directly calculated from the TB wave functions, as detailed in Refs. [61, 36].

In the discussions presented in Sec. 4.1, we pointed out that hole states are strongly affected in the presence of alloy fluctuations and the energy level splitting of hole states is smaller as compared to electrons. Additionally, it was noted that the energetic difference between hole states also varies between configurations. Therefore, it is not immediately clear how different configurations will be affected by randomness in the alloy. If energetic difference between the hole states are small, one could expect that more hole states will have to be taken into account in the CI expansion to obtain accurate results for the FSS values. Keeping this in mind, we include more hole states (first ten states) in our CI framework. For the electrons we include the six energetically lowest single-particle states. We stress that we are mainly interested in how the alloy microstructure affects the symmetry and degeneracies of the excitonic states. For this purpose the above outlined approach is sufficient.

Finally, once the many-body Hamiltonian is

constructed and diagonalized, the resulting many-body states are used to calculate optical spectra. This is done via Fermi's Golden Rule; the required dipole matrix elements are again directly obtained from the TB wave functions. In this work we have restricted the dipole matrix element calculation to the envelope part, since again we are mainly interested in symmetry properties of the allowed transitions and not the absolute magnitude. For such a purpose the envelope part is sufficient. More details about the calculations of the dipole matrix elements and emission/absorption spectra can be found elsewhere. [61, 38]


[1] Gisin N, Ribordy G, Tittel W and Zbinden H 2002 *Rev. Mod. Phys.* **74**(1) 145–195

[2] Kimble H J 2008 *Nature* **453** 1023–1030 ISSN 1476-4687

[3] Huber D, Reindl M, Aberl J, Rastelli A and Trotta R 2018 *Journal of Optics* **20** 073002

[4] Orieux A, Versteegh M A M, Jns K D and Ducci S 2017 *Reports on Progress in Physics* **80** 076001

[5] Horn R, Abolghasem P, Bijlani B J, Kang D, Helmy A S and Weihs G 2012 *Phys. Rev. Lett.* **108**(15) 153605

[6] Di Giuseppe G, Atatüre M, Shaw M D, Sergienko A V, Saleh B E A and Teich M C 2002 *Phys. Rev. A* **66**(1) 013801

[7] Zhang H, Jin X M, Yang J, Dai H N, Yang S J, Zhao T M, Rui J, He Y, Jiang X, Yang F, Pan G S, Yuan Z S, Deng Y, Chen Z B, Bao X H, Chen S, Zhao B and Pan J W 2011 *Nature Photonics* **5** 628–632 ISSN 1749-4893

[8] Akopian N, Lindner N H, Poem E, Berlatzky Y, Avron J, Gershoni D, Gerardot B D and Petroff P M 2006 *Phys. Rev. Lett.* **96**(13) 130501

[9] Muller A, Fang W, Lawall J and Solomon G S 2009 *Phys. Rev. Lett.* **103**(21) 217402

[10] Plumhof J D, Trotta R, Rastelli A and Schmidt O G 2012 *Nanoscale Res. Lett.* **7** 336

[11] Bester G, Nair S and Zunger A 2003 *Phys. Rev. B* **67**(16) 161306

[12] Dupertuis M A, Karlsson K F, Oberli D Y, Pelucchi E, Rudra A, Holtz P O and Kapon E 2011 *Phys. Rev. Lett.* **107**(12) 127403

[13] Karlsson K F, Dupertuis M A, Oberli D Y, Pelucchi E, Rudra A, Holtz P O and Kapon E 2010 *Phys. Rev. B* **81**(16) 161307

[14] Juska G, Dimastrodonato V, Mereni L O, Gocalinska A and Pelucchi E 2013 *Nature Photonics* **7** 527

[15] Baer N, Schulz S, Gartner P, Schumacher S, Czycholl G and Jahnke F 2007 *Phys. Rev. B* **76**(7) 075310

[16] Schulz S, Caro M A, O'Reilly E P and Marquardt O 2011 *Phys. Rev. B* **84**(12) 125312

[17] Moses P G, Miao M, Yan Q and Van de Walle C G 2011 *J. Chem. Phys.* **134** 084703

[18] Pelekanos N T, Dialynas G E, Simon J, Mariette H and Daudin B 2005 *Journal of Physics: Conference Series* **10** 61–68

[19] Patra S K and Schulz S 2016 *Journal of Physics D: Applied Physics* **50** 025108

[20] Holmes M J, Choi K, Kako S, Arita M and Arakawa Y 2014 *Nano Lett.* **14** 982

[21] Holmes M J, Kako S, Choi K, Arita M and Arakawa Y 2016 *ACS Photonics* **3** 543–546

[22] Wang T, Puchtler T J, Patra S K, Zhu T, Jarman J C, Oliver R A, Schulz S and Taylor R A 2017 *Scientific Reports* **7** 12067 ISSN 2045-2322

[23] Yang W, Li J, Zhang Y, Huang P K, Lu T C, Kuo H C, Li S, Yang X, Chen H, Liu D and Kang J 2014 *Scientific Reports* **4** 5166 ISSN 2045-2322

[24] Graham D M, Soltani-Vala A, Dawson P, Godfrey M J, Smeeton T M, Barnard J S, Kappers M J, Humphreys C J and Thrush E J 2005 *J. Appl. Phys.* **97** 103508

[25] Dawson P, Schulz S, Oliver R A, Kappers M J and Humphreys C J 2016 *J. Appl. Phys.* **119** 181505

[26] Williams D P, Andreev A D, O'Reilly E P and Faux D A 2005 *Phys. Rev. B* **72**(23) 235318

[27] Caro M A, Schulz S and O'Reilly E P 2013 *Phys. Rev. B* **88**(21) 214103

[28] Wimmer M, Nair S V and Shumway J 2006 *Phys. Rev. B* **73**(16) 165305

[29] Woodward J M, Nikiforov A Y, Ludwig K F and Moustakas T D 2017 *J. Appl. Phys.* **122** 065305

[30] Oliver R A, Briggs G A D, Kappers M J, Humphreys C J, Yasin S, Rice J H, Smith J D and Taylor R A 2003 *Appl. Phys. Lett.* **83** 755–757

[31] Jarjour A F, Oliver R A, Tahraoui A, Kappers M J, Humphreys C J and Taylor R A 2007 *Phys. Rev. Lett.* **99**(19) 197403

[32] Tsai W, Hong K and Kuo M 2010 *Phys. Status Solidi (b)* **247** 1764–1768

[33] Hong K B and Kuo M K 2010 *Semicond. Sci. Tech.* **25** 065005

[34] Humphreys C, Griffiths J, Tang F, Oehler F, Findlay S, Zheng C, Etheridge J, Martin T, Bagot P, Moody M, Sutherland D, Dawson P, Schulz S, Zhang S, Fu W, Zhu T, Kappers M and Oliver R 2017 *Ultramicroscopy* **176** 93 – 98

[35] Butt R, Lahourcade L, Udavinys T K, Callsen G, Mensi M, Glauser M, Rossbach G, Martin D, Carlin J F, Marcinkeviius S and Grandjean N 2018 *Applied Physics Letters* **112** 032106

[36] Patra S K 2020 *Electronic and optical properties of III-Nitride nanostructures* Ph.D. thesis University College Cork

[37] Andreev A D and O'Reilly E P 2000 *Phys. Rev. B* **62** 15851

[38] Schulz S, Schumacher S and Czycholl G 2008 *The European Physical Journal B* **64** 51–60 ISSN 1434-6036

[39] Tomić S and Vukmirović N 2009 *Phys. Rev. B* **79**(24) 245330

[40] Schulz S 2007 *Electronic and Optical Properties of Quantum Dots: A Tight?Binding Approach* Ph.D. thesis University of Bremen

[41] Baer N, Schulz S, Schumacher S, Gartner P, Czycholl G and Jahnke F 2005 *Appl. Phys. Lett.* **87** 231114

[42] Williamson A J, Wang L W and Zunger A 2000 *Phys. Rev. B* **62**(19) 12963–12977

[43] Vurgaftman I and Meyer J R 2003 *Journal of Applied Physics* **94** 3675–3696

[44] Schliwa A, Winkelnkemper M and Bimberg D 2007 *Phys. Rev. B* **76**(20) 205324

[45] Nishat M R K and Ahmed S S 2020 *IEEE Journal of Quantum Electronics* **56** 1–9

[46] Schulz S, Caro M A, Coughlan C and O'Reilly E P 2015 *Phys. Rev. B* **91** 035439

[47] Auf der Maur M, Pecchia A, Penazzi G, Rodrigues W and Di Carlo A 2016 *Phys. Rev. Lett.* **116** 027401

[48] Jones C M, Teng C H, Yan Q, Ku P C and Kioupakis E 2017 *Appl. Phys. Lett.* **111** 113501

[49] Altmann S L and P H 1994 *Point-Group Theory Tables* (Clarendon Press)

[50] Tanner D S P, Caro M A, O'Reilly E P and Schulz S 2016 *RSC Adv.* **6**(69) 64513–64530

[51] Tanner D S, Dawson P, Kappers M J, Oliver R A and Schulz S 2020 *Phys. Rev. Applied* **13**(4) 044068

[52] Vurgaftman I, Meyer J R and Ram-Mohan L R 2001 *Journal of Applied Physics* **89** 5815–5875

[53] Beljonne D, Shuai Z, Pourtois G and Bredas J L 2001 *The Journal of Physical Chemistry A* **105** 3899–3907

[54] Verma J, Islam S M, Protasenko V, Kumar Kandaswamy P, (Grace) Xing H and Jena D 2014 *Applied Physics Letters*

**104** 021105
[55] Amloy S, Moskalenko E S, Eriksson M, Karlsson K F, Chen Y T, Chen K H, Hsu H C, Hsiao C L, Chen L C and Holtz P O 2012 *Appl. Phys. Lett.* **101** 061910
[56] Jemsson T, Machhadani H, Holtz P O and Karlsson K F 2015 *Nanotechnology* **26** 065702
[57] Cho J H, Kim Y M, Lim S H, Yeo H S, Kim S, Gong S H and Cho Y H 2018 *ACS Photonics* **5** 439
[58] Tang F, Zhu T, Fu W Y, Oehler F, Zhang S, Griffiths J T, Humphreys C, Martin T L, Bagot P A J, Moody M P, Patra S K, Schulz S, Dawson P, Church S, Jacobs J and Oliver R A 2019 *Journal of Applied Physics* **125** 225704
[59] Jayakumar H, Predojević A, Kauten T, Huber T, Solomon G S and Weihs G 2014 *Nature Communications* **5** 4251 ISSN 2041-1723
[60] Patra S K and Schulz S 2020 *Nano Letters* **20** 234–241 ISSN 1530-6984
[61] Schulz S, Schumacher S and Czycholl G 2006 *Phys. Rev. B* **73**(24) 245327
[62] Schulz S, Caro M A, Tan L T, Parbrook P J, Martin R W and O'Reilly E P 2013 *Appl. Phys. Express* **6** 121001
[63] Coughlan C, Schulz S, Caro M A and OReilly E P 2015 *Phys. Status Solidi B* **252** 879
[64] Chadi D J 1977 *Phys. Rev. B* **16**(2) 790–796
[65] Li Z Q and Pötz W 1992 *Phys. Rev. B* **46** 2109
[66] O'Reilly E P, Lindsay A, Tomic S and Kamal-Saadi M 2002 *Semicond. Sci. Technol.* **17** 870
[67] Boykin T B, Kharche N, Klimeck G and Korkusinski M 2007 *J. Phys.: Condens. Matter* **19** 036203
[68] Kobayashi A, Sankey O F, Volz S M and Dow J D 1983 *Phys. Rev. B* **28**(2) 935–945
[69] Martin R M 1970 *Phys. Rev. B* **1** 4005